

# Squeezed state purification with linear optics and feed forward

O. Glöckl<sup>1,\*</sup>, U. L. Andersen<sup>1</sup>, R. Filip<sup>1,2</sup>, W. P. Bowen<sup>3</sup>, and G. Leuchs<sup>1</sup>

<sup>1</sup> *Institut für Optik, Information und Photonik, Max-Planck Forschungsgruppe, Universität Erlangen-Nürnberg, Günther-Scharowsky-Straße 1 / Bau 24, 91058 Erlangen, Germany*

<sup>2</sup> *Department of Optics, Palacky University, Olomouc, Czech Republic,*

<sup>3</sup> *Department of Physics, University of Otago, Dunedin, New Zealand*

(Dated: August 27, 2018)

A scheme for optimal and deterministic linear optical purification of mixed squeezed Gaussian states is proposed and experimentally demonstrated. The scheme requires only linear optical elements and homodyne detectors, and allows the balance between purification efficacy and squeezing degradation to be controlled. One particular choice of parameters gave a ten-fold reduction of the thermal noise with a corresponding squeezing degradation of only 11 %. We prove optimality of the protocol, and show that it can be used to enhance the performance of quantum informational protocols such as dense coding and entanglement generation.

PACS numbers: 42.50.Dv, 42.50.Lc, 03.67.Hk

Quantum information science facilitates many information processing tasks that were previously thought intractable or impossible [1]. Without exception, however, these protocols are highly susceptible to decoherence and impurities [2]. As a result, significant effort has been put into developing procedures to purify the required non-classical resources. It has recently been shown that perfect single photon purification is impossible using only linear optics, rendering the protocol rather challenging [3]. Nevertheless, techniques to non-deterministically purify single photon states (as a resource) have been proposed both when a single copy and two copies are available [4], but so far, no experiments have been reported. Here, we examine the complementary problem of purification of continuous variable (CV) states, in particular Gaussian squeezed states. We find that in this regime, in contrast to the single photon case, purification of CV resource states is indeed achievable with linear optics.

Gaussian squeezed states are an essential resource for deterministic quantum information processing; allowing the immediate generation of CV entanglement [5], and facilitating a variety of important protocols such as unconditional quantum teleportation [6], dense coding [7], and entanglement swapping [8]. The efficacy of these protocols typically depends critically on both the degree of squeezing and the purity of the squeezed states. Presently available squeezed states are often highly impure (i.e. mixed) due to decoherence and dissipation in the preparation sources. It is therefore important to develop effective purification techniques for these states. In this paper, we determine the optimal level of purification possible for single Gaussian squeezed states, propose an experiment that achieves this level, and perform an experimental demonstration. In contrast to single photon purification, the protocol is deterministic, which presents significant advantages in terms of scalability and reliability in compound quantum information protocols. Additionally, although the past decade has seen significant improvements in the degree of squeezing achievable by experimentalists [9], the work present here represents the

first experiment dedicated to improving purity.

The purity of a Gaussian squeezed state is given simply by  $\text{tr}(\rho^2) = 1/\sqrt{\Delta^2\hat{X} \cdot \Delta^2\hat{Y}}$  [10], where  $\Delta^2\hat{X}$  and  $\Delta^2\hat{Y}$  are the variances of the squeezed [ $\hat{X} = \hat{a}^\dagger + \hat{a}$ ] and the anti-squeezed [ $\hat{Y} = i(\hat{a}^\dagger - \hat{a})$ ] quadratures, respectively, and  $\rho$  is the density matrix. A maximally pure state has  $\text{tr}(\rho^2) = 1$ , however, in realistic systems the purity is typically much worse. In fibre based systems, for example, guided-acoustic-wave Brillouin scattering causes  $\text{tr}(\rho^2)$  to be typically smaller than 0.1 [11]. Experimentally feasible squeezed state purification techniques that do not require non-linear interactions or non-classical ancilla states are vital for these states to be useful in quantum information systems.

In the Heisenberg picture a generic Gaussian operation can be described by the linear transformations [12]

$$\hat{X}' = \nu\hat{X} + \hat{X}_N, \quad \hat{Y}' = \mu\hat{Y} + \hat{Y}_N, \quad (1)$$

where  $\nu, \mu \in \Re$ , and  $\hat{X}_N$  and  $\hat{Y}_N$  are operators associated with noise added by the device in the amplitude and phase quadratures, respectively. We see from the form of  $\text{tr}(\rho^2)$  that the optimal purification technique must minimize  $\Delta^2\hat{Y}'$  whilst minimally disturbing the degree of squeezing  $\Delta^2\hat{X}'$ . Let us therefore identify the minimum achievable  $\Delta^2\hat{Y}'$  for a given  $\Delta^2\hat{X}'$ . Assuming no correlations between the input and noise operators, the amplitude and phase quadrature variances of the purified state are given by

$$\Delta^2\hat{X}' = \nu^2\Delta^2\hat{X} + \Delta^2\hat{X}_N, \quad \Delta^2\hat{Y}' = \mu^2\Delta^2\hat{Y} + \Delta^2\hat{Y}_N. \quad (2)$$

From (1) and the quadrature operator commutation relations ( $[X, Y] = [X', Y'] = 2i$ ) we also find  $[X_N, Y_N] = 2i(1 - \nu\mu)$  and thus the uncertainty relation  $\Delta^2\hat{X}_N\Delta^2\hat{Y}_N \geq (1 - \nu\mu)^2$ . A lower bound on  $\Delta^2\hat{Y}'$  can be obtained from the saturation of this inequality and Eqs. (2)[20]

$$\Delta^2\hat{Y}'_{\min}(\nu, \mu) = \frac{(1 - \nu\mu)^2}{\Delta^2\hat{X}' - \nu^2\Delta^2\hat{X}} + \mu^2\Delta^2\hat{Y}. \quad (3)$$

Our goal is to determine the minimum of Eq. (3) with respect to  $\nu$  and  $\mu$ , achievable using linear transformations. The range of  $\nu$  can be constrained. From Eqs. (2) we have  $\nu^2 < \Delta^2\hat{X}'/\Delta^2\hat{X}$ . Furthermore, since only linear operations are allowed an input coherent state cannot be output squeezed. As a result  $\Delta^2\hat{X}_N \geq 1 - \nu^2$ , and therefore  $\nu^2 \geq (1 - \Delta^2\hat{X}')/(1 - \Delta^2\hat{X})$ . The minimum of Eq. (3) can be found by first minimizing over  $\mu$ . It is then easy to see that the minimum within our constraints on  $\nu$  occurs at the lower bound with  $\nu^2 = (1 - \Delta^2\hat{X}')/(1 - \Delta^2\hat{X})$ , and we find

$$\Delta^2\hat{Y}'_{\min} = \frac{\Delta^2\hat{Y}(1 - \Delta^2\hat{X})}{(1 - \Delta^2\hat{X}') + \Delta^2\hat{Y}(\Delta^2\hat{X}' - \Delta^2\hat{X})}. \quad (4)$$

This expression determines the optimal solution for a deterministic linear purification scheme [21].

Let us now consider the optimality of the purification scheme shown in Fig. 1. The basic idea is to use homodyne detection and electro optic feed forward to control the quantum fluctuations similar to earlier work reported e. g. in [14]. A fraction  $\sqrt{1-\eta}$  of the amplitude squeezed input mode  $\hat{a}$  is tapped off at a variable beam splitter consisting of a polarizing beam splitter and a half-wave plate. The (anti-squeezed) phase quadrature of the reflected beam  $\hat{r}$  is measured. The resulting measurement outcome is amplified by a gain factor  $g$ , and fed forward onto the transmitted mode  $\hat{t}$  using a phase modulator. By optimizing the gain a minimum phase quadrature variance of  $\Delta^2\hat{Y}_{t,\min} = \Delta^2\hat{Y}_a/(\eta + (1-\eta)\Delta^2\hat{Y}_a)$  can be achieved for the transmitted beam, where  $\Delta^2\hat{Y}_a$  denotes the phase quadrature variance of the input. Since the amplitude and phase quadratures are orthogonal, the feed-forward will not affect the amplitude quadrature of the transmitted mode, the variance of which is therefore simply  $\Delta^2\hat{X}_t = \eta\Delta^2\hat{X}_a + 1 - \eta$ . Solving this relation for  $\eta$  and substituting into the relation for  $\Delta^2\hat{Y}_{t,\min}$  we find that this device delivers the desired optimum performance described by (4).

In our experiment, we use intense amplitude squeezed beams from a fibre Sagnac interferometer [15]. To perform phase quadrature measurements we use an asymmetric Mach Zehnder interferometer [16] which translates phase noise into directly detectable amplitude noise at a specific sideband frequency. Amplitude noise measurements are accomplished by rotating the input polarization by  $45^\circ$ , thus bypassing the interferometer.

Since all involved states are Gaussian, the performance of the device is fully characterized by measuring the variances  $\Delta^2\hat{X}_t$  and  $\Delta^2\hat{Y}_t$  of the transmitted state. These variances are measured using interferometer II with and without the use of the feed-forward loop. The results and theoretical predictions are plotted as a function of the transmission  $\eta$  in Fig. 2. The overall detection efficiency  $\eta_{\text{Det}}$  of the Mach Zehnder interferometers used for phase measurement was around 70% due to imperfect photo diodes, interference contrast, and losses in optical components. Non-unity detection efficiency affects

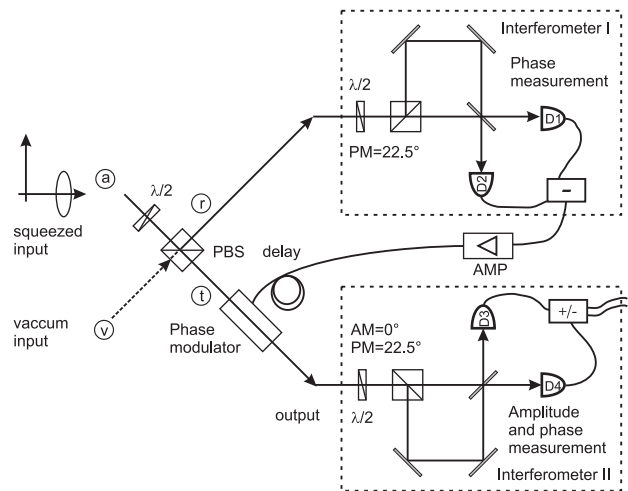


FIG. 1: Experimental setup of the phase noise subtraction scheme. A fraction of input mode  $\hat{a}$  is tapped off to perform phase quadrature measurements using interferometer I. The resulting photocurrent is amplified (AMP) and, after introducing an appropriate cable delay, fed forward to the modulator. The amplitude and phase noise of the transmitted mode is characterized by interferometer II. AMP: electrical amplifier, PBS: Polarizing beam splitter,  $\lambda/2$ : Half wave plate.

the detected noise levels. As the measured quantities in both cases (that is, with and without feed forward) are well above the shot noise limit the vacuum noise contribution due to the inefficiency can be neglected, and the measured variances therefore almost exactly scale with the efficiency of the verification stage. Hence, the ratio  $\Delta^2\hat{Y}_t/\Delta^2\hat{Y}_{t,\min}$  yields a measure of the excess noise reduction that is to good approximation independent of the detection efficiency. When the introduction of vacuum noise is taken into account, we see that any degradation of the detection efficiency can only result in an underestimation of the level of purification.

The experimentally observed phase quadrature variance of the transmitted beam is shown in Fig. 2a. When the feed-forward was switched off (filled squares), the phase quadrature variance  $\Delta^2\hat{Y}_t$  decreased linearly as the transmission was reduced simply due to the beam splitter attenuation. The solid line shows the expected behavior of the measured phase noise as a function of  $\eta$ . When the feed-forward was active (open circles) the behavior changed dramatically, with the phase quadrature variance  $\Delta^2\hat{Y}_{t,\min}$  decreasing much more rapidly. The predicted behavior is plotted as a function of transmission (gray solid line). The detection efficiency of interferometer I limits the performance of the scheme (indicated by the dashed gray line). During the measurement run, the visibility, and hence the detection efficiency of interferometer II, gradually degraded. Finally, at a transmission  $\eta = 0.81$ , interferometer II was realigned giving rise to a discontinuity in the measured noise levels. However, as can be seen from the enlargement of Fig. 2a and as discussed above, the purification process is to good ap-

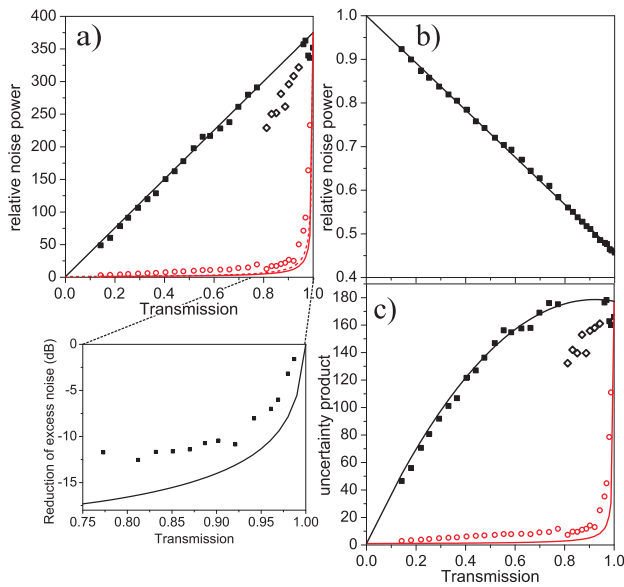


FIG. 2: Experimental results as a function of transmission. a) and b): phase and amplitude quadrature variances of the transmitted beam, c): product of phase and amplitude quadrature variances. Open circles and filled squares represent the results with and without feed-forward, respectively; open diamonds in a) represent values taken at reduced detection efficiency (cf. main text). Also plotted is the degree of excess noise reduction which is independent of the actual detection efficiency. The lines are obtained from our theoretical model, with the dashed line in a) taking into account nonunit phase quadrature measurement efficiency of mode  $\hat{r}$ . All variances were normalized to the shot noise level. Measurement frequency: 20.5 MHz. Electronic noise of  $-83.3$  dBm, was subtracted from the measured data.

proximation independent of detection efficiency, and can certainly not be enhanced by worsening efficiency.

Fig. 2b shows the amplitude quadrature variance  $\Delta^2 \hat{X}_t$  as a function of transmission. The level of squeezing decreases linearly as  $\eta$  is reduced, as is typical of squeezed states upon attenuation. As expected, identical behavior was observed with and without feed-forward. From the interpolated variance at  $\eta \rightarrow 0$  and that measured at  $\eta = 1$ , we conclude that 3.4 dB of squeezing was present in the detected input field.

The uncertainty product (which is directly related to the purity) of the transmitted state is plotted as a function of  $\eta$  in Fig. 2c. The open circles and filled squares correspond to the experimental results with and without the use of feedforward, respectively. The expected theoretical behavior is again plotted for both cases, and agrees well with the experimental results. It is clear that the purity can be increased considerably, even for quite high transmission ( $> 90\%$ ). When  $\eta = 0.92$ , for example, the purity is improved by more than an order of magnitude, while the squeezing is only degraded by 11% from  $\Delta^2 \hat{X}_t = 0.47$  to  $\Delta^2 \hat{X}_t = 0.52$ .

Mechanisms that produce squeezed states of light rely

on the generation of photons in correlated pairs. This photon pairing is responsible for the non-classicality of the states, while impurity is caused by unpaired photons. From this perspective, the effect of our purification scheme is to selectively remove unpaired (thermal) photons, while retaining the maximal number of pairs. This process is visualized on the photon number diagram in Fig. 3, where the mean number of non-classical  $\langle \hat{n} \rangle_{\text{non-cl}}$  and thermal  $\langle \hat{n} \rangle_{\text{thermal}}$  photons per bandwidth per time are calculated from  $\langle \hat{n} \rangle_{\text{non-cl}} = (\Delta^2 \hat{X}_{\text{sqz}} + 1 / \Delta^2 \hat{X}_{\text{sqz}} - 2) / 4$  and  $\langle \hat{n} \rangle_{\text{thermal}} = \langle \hat{n} \rangle_{\text{total}} - \langle \hat{n} \rangle_{\text{non-cl}}$ , respectively, and the total mean photon number per bandwidth per time is  $\langle \hat{n} \rangle_{\text{total}} = (\Delta^2 \hat{X} + \Delta^2 Y - 2) / 4$  [17]. The effect of purification is clearly seen. The number of thermal photons per bandwidth per time drops rapidly with only a very small corresponding change in the number of non-classical photons. One benefit of the photon number diagram is that efficacy contours can be plotted for quantum information processes. In our case this enables the tap-off fraction  $\sqrt{1 - \eta}$  to be chosen to ensure that the quantum resources are optimally configured to suit the quantum information protocol they will be utilized for.

The purification scheme investigated in this paper is particularly useful for protocols where the total number of photons is a critical resource. One example of such is dense coding, where entanglement is utilized to enhance the capacity of an information channel to beyond the Holevo limit [18]  $C_{\text{Holevo}} = [1 + \langle \hat{n} \rangle_{\text{cp}}] \log_2 [1 + \langle \hat{n} \rangle_{\text{cp}}] - \langle \hat{n} \rangle_{\text{cp}} \log_2 \langle \hat{n} \rangle_{\text{cp}}$  where  $\langle \hat{n} \rangle_{\text{cp}}$  is the mean total number of photons per bandwidth per time used in the communication process. The channel capacity of the continuous variable dense coding protocol [7] is given by [17]

$$C_{\text{EPR}} = \log_2 \left[ 1 + \frac{\langle \hat{n} \rangle_{\text{signal}}}{2 \langle \hat{n} \rangle_{\text{non-cl}} + 1 - 2 \sqrt{\langle \hat{n} \rangle_{\text{non-cl}}^2 + \langle \hat{n} \rangle_{\text{non-cl}}}} \right]$$

with  $\langle \hat{n} \rangle_{\text{signal}} = \langle \hat{n} \rangle_{\text{cp}} - \langle \hat{n} \rangle_{\text{thermal}} - \langle \hat{n} \rangle_{\text{non-cl}}$  [22]. In the limit that  $\langle \hat{n} \rangle_{\text{cp}} = \langle \hat{n} \rangle_{\text{signal}} + \langle \hat{n} \rangle_{\text{total}} \gtrsim \langle \hat{n} \rangle_{\text{thermal}}$ ,  $C_{\text{EPR}}$  is highly sensitive to the level of impurity ( $\langle \hat{n} \rangle_{\text{thermal}}$ ) present in the system. Dense coding channel capacity contours for  $\langle \hat{n} \rangle_{\text{cp}} = 400$  are shown in Fig. 3. The degradation in channel capacity caused by thermal photons can be seen directly from the slant of the contours.

Examining the dense coding efficacy contours near our experimental data points, we see that with no purification the optimal channel capacity achievable with our squeezing is  $C_{\text{EPR}} \approx 0.925 C_{\text{clas}}$ . Employing the purification scheme this is enhanced to  $C_{\text{EPR}} \approx 0.95 C_{\text{clas}}$ . Even though the channel capacity is improved, the dense coding protocol remains unsuccessful ( $C_{\text{EPR}} < C_{\text{clas}}$ ). However, the effectiveness of our scheme when applied to dense coding can be judged from the trajectories labelled b) in Fig. 3. In this case, we consider squeezed resources with  $\Delta^2 \hat{X}_{\text{sqz}} = 0.3$  and  $\Delta^2 \hat{Y}_{\text{anti}} = 400$ . The threshold for successful dense coding can then be easily surpassed. Therefore, our purification scheme can be used to transform quantum resources from a form for

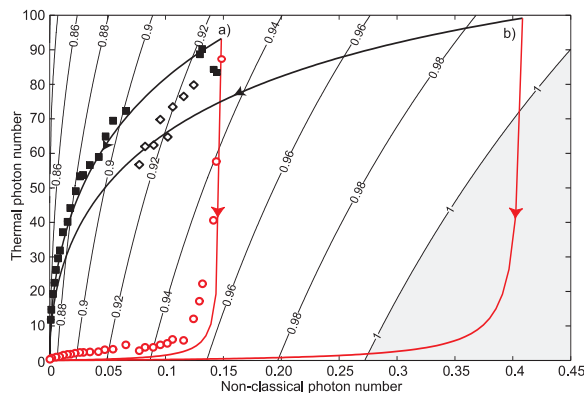


FIG. 3: Photon number diagram showing experimental purification results and ideal purification trajectories. a) ideal trajectory for initial state used in experiments. b) trajectory for initial state with  $\Delta^2 \hat{X}_{sqz} = 0.3$  and  $\Delta^2 \hat{Y}_{anti} = 400$ . Dark trajectories/points: no feed-forward. Light trajectories/points: feed-forward. The contours represent lines of constant  $C_{EPR}$  for  $\langle \hat{n} \rangle_{cp} = 400$ , normalized to  $C_{Holevo}$ . Shading indicates the region in which dense coding is successful.

which dense coding is not possible, into a form which allows for its successful implementation.

Let us look at another interesting aspect of the purification scheme. The entanglement generated by the interference of two squeezed beams on an asymmetric beam splitter can be characterized in terms of the entanglement

of formation if the covariance matrix is transformed into the normal form [19]. If a perfectly symmetric beam splitter is used to generate entanglement, the entanglement of formation is independent of the purity of the squeezed states. In realistic systems however, the beam splitting ratio is not perfectly symmetric and in that case, the generated correlations depend on the purity of the squeezed input states. For very asymmetric beam splitting ratios and for squeezed beams with high excess noise levels we find that the degree of entanglement quite surprisingly can be increased by purifying the squeezed resources despite the fact that less squeezing is actually available after purification.

In summary, we have presented and demonstrated an optimal linear optics and homodyne detection based purification scheme to remove thermal noise from squeezed states. Over an order of magnitude of thermal noise reduction was achieved with a corresponding reduction in squeezing of only 11 %. This protocol is useful for quantum information protocols such as dense coding and entanglement swapping, and can enhance the levels of entanglement available in realistic systems.

We thank T. C. Ralph and C. Silberhorn for useful discussions. The work was supported by the EU project COVAQIAL (No. FP6-511004). R.F. acknowledges support from the projects GACR 202/03/D239, MSM6198959213 and the Alexander von Humboldt foundation. W.P.B. acknowledges funding from the MacDiarmid Institute.

\* Electronic address: gloeckl@kerr.physik.uni-erlangen.de; present address: ARC Centre of Excellence for Quantum Atom Optics, The Australian National University, Canberra ACT 0200, Australia

- [1] M.A. Nielsen and I.L. Chuang, *Quantum Computation and Quantum Information*, Cambridge University Press (2000).
- [2] P. Kok et al., quant-ph/0512071; N. Gisin et al., Rev. Mod. Phys. **74**, 145 (2002).
- [3] D. W. Berry et al., Phys. Rev. A **69**, 031806(R) (2004).
- [4] See e. g. W. J. Munro et al. Phys. Rev. A **71**, 033819 (2005); T. Konrad et al., quant-ph/0510113
- [5] G. Yeoman, S.M. Barnett, J. Mod. Optics, **40**, 1497 (1993); T.C. Ralph and P.K. Lam, Phys. Rev. Lett. **81**, 5668 (1998); G. Leuchs, T.C. Ralph, C. Silberhorn et al., J. Mod. Opt. **46**, 1927 (1999).
- [6] L. Vaidman, Phys. Rev. A **49**, 1473 (1994); S. L. Braunstein and H. J. Kimble, Phys. Rev. Lett. **80**, 869 (1998); A. Furusawa et al., Science **282**, 706 (1998).
- [7] J. Ban, J. Opt. B **1**, L9 (1999); S. L. Braunstein and H. J. Kimble, Phys. Rev. A **61**, 042302 (2000); X. Li et al., Phys. Rev. Lett. **88**, 047904 (2002);
- [8] P. van Loock and S. L. Braunstein, Phys. Rev. A **61**, 010302(R) (1999); X. Jia et al., Phys. Rev. Lett. **93**, 250503 (2004); N. Takei, et al., Phys. Rev. Lett. **94**, 220502 (2005).
- [9] H. Bachor and T.C. Ralph, *A Guide to Experiments in Quantum Optics*, WILEY-VCH Verlag GmbH & Co.,

Weinheim, (2004).

- [10] M. G. A. Paris et al., Phys. Rev. A **68**, 012314 (2003).
- [11] R. M. Shelby et al., Phys. Rev. Lett. **57**, 691 (1986).
- [12] A. S. Holevo, Prob. Inf. Trans. **8**, 63 (1972).
- [13] B. C. Buchler et al., Phys. Rev. A **60**, 529, (1999).
- [14] J. Mertz et al., Phys. Rev. Lett. **64**, 2897 (1990); P. K. Lam et al., Phys. Rev. Lett. **79**, 1471 (1997).
- [15] S. Schmitt et al., Phys. Rev. Lett. **81**, 2446 (1998); D. Krylov and K. Bergman, Opt. Lett. **23**, 1390 (1998); M. Fiorentino et al., Phys. Rev. A **64**, 031801(R) (2001).
- [16] O. Glöckl et al., Opt. Lett. **29**, 1936 (2004).
- [17] W. P. Bowen et al., Phys. Rev. Lett. **90**, 043601 (2003); W. P. Bowen et al., Phys. Rev. A **69**, 012304 (2004).
- [18] C. M. Caves and P. D. Drummond, Rev. Mod. Phys. **66**, 481 (1994); T. C. Ralph and E. H. Huntington, Phys. Rev. A **66**, 042321 (2002).
- [19] G. Giedke et al., Phys. Rev. Lett. **91**, 107901 (2003).
- [20] It is assumed here that  $\Delta^2 \hat{X}_N \neq 0$ .
- [21] Another potential solution for  $\Delta^2 \hat{Y}'$  exists for  $\Delta^2 \hat{X}_N = 0$  (this corresponds to noiseless amplification [13]). However, the solution is worse than that found in Eq. (4).
- [22] We assume that the entanglement is produced by two identical squeezed beams. Therefore, the terms used here are related to those used in [17] as follows:  $2\langle \hat{n} \rangle_{non-cl} = \bar{n}_{min}$ ,  $2\langle \hat{n} \rangle_{thermal} = \bar{n}_{excess}$ ,  $\langle \hat{n} \rangle_{cp} = \bar{n}_{encoding}$ ,  $2\langle \hat{n} \rangle_{total} = \bar{n}_{total}$ . The factors of two arise because photon numbers here are calculated for a single squeezed beam, whereas in [17] they represent the entire entangled system.